(accepted)
Journal of Physics D: Applied Physics 55(27). p.-.275106

# Enhancing laser-nanoparticle interactions by diffused laser beams: efficient size-reduction of nanoparticles

**XINYUE ZHENG,[a] KOTA ANDO,[a] XIAOLONG WANG,[b] TETSUO SAKKA,[c] AND TAKASHI NAKAJIMA[a,*]**

[a] *Institute of Advanced Energy, Kyoto University, Gokasho, Uji, Kyoto 611-0011, Japan*
[b] *Department of Applied Physics, Zhejiang University of Technology, Hangzhou, 310023, China*
[c] *Department of Energy and Hydrocarbon Chemistry, Kyoto University, Kyoto 615-8510, Japan*
**Corresponding author: nakajima@iae.kyoto-u.ac.jp*

Received XX Month XXXX; revised XX Month, XXXX; accepted XX Month XXXX; posted XX Month XXXX (Doc. ID XXXXX); published XX Month XXXX

**Generally speaking, a laser beam with a good spatial profile such as flat-top or Gaussian ($TEM_{00}$ mode) shape is considered to be a prerequisite to maximize laser-matter interactions. On the contrary, we show that, if the process of interest has a threshold in terms of laser fluence or intensity, a diffused laser beam can do a good job to induce the process. As an example we demonstrate the efficient size-reduction of colloidal nanoparticles by a diffused laser beam and identify that the physical origin of this counterintuitive results is a redistribution of laser energy, i.e., formation of speckles through a diffuser where the local laser fluence exceeds the size-reduction threshold. We report the systematic results for silver and gold nanoparticles.**

## 1. Introduction

Applying the laser-based techniques to synthesize nanoparticles (NPs) and/or alter their various properties is a rapidly growing field in recent years. Among them, laser ablation in liquid (LAL) is a very simple and versatile technique to synthesize NPs [1,2]. Its drawback, however, is that LAL-synthesized NPs usually exhibit a polydisperse size distribution. This is because primary NPs produced by LAL are exposed to the explosive boiling or coalescence to result in larger secondary NPs [3]. To solve this problem an introduction of the second laser with a modest laser fluence has been proposed [4], where its role is to induce size-reduction or equivalently fragmentation of secondary NPs, leading to the significant improvement of particle size distribution. Obviously a simpler and more efficient way to promote the size-reduction of NPs is highly desired [5,6].

In many cases the spatial mode of a laser beam is considered to be very important to attain the maximum laser-matter interactions, and this is why a flat-top or Gaussian ($TEM_{00}$ mode) beam is widely used. While this is generally true it is not prerequisite in some circumstances. As an example, we consider the laser induced size-reduction of colloidal NPs mentioned above. Upon irradiation of a laser pulse colloidal NPs absorb the laser energy and the NP temperature increases (photothermal effect). If the laser fluence is beyond the size-reduction *threshold*, then the temperature increase is so much that melting and even evaporation of NPs occurs to break up [7–14]. This is the brief description of laser induced size-reduction of colloidal NPs, and two scenarios have been proposed to explain this phenomenon. They are photothermal melting (that may be further accompanied by evaporation) of NPs [9,15] and Coulomb explosion [10,13,16,17] as a result of multiple electron ejection without electronic relaxation of the multiply ionized core, where the former and the latter are more likely to occur by relatively long (nanosecond) and short (picosecond or femtosecond) laser pulses, respectively. Knowing that what matters for the size-reduction of NPs is whether the local laser fluence *at the locations of NPs* exceeds the size-reduction threshold or not, we realize that using a flat-top or Gaussian laser beam may not be a prerequisite for the efficient size-reduction of NPs, and similar must be true for other processes such as reshaping of NPs [15,18,19] as well as nanorods (NRs) [20–22], synthesis of bimetallic NPs [23–25], and welding of nanowires [26], since certain laser fluence thresholds exist for all those processes.

To demonstrate what we mean, we irradiate the colloidal silver nanoparticles (Ag NPs) (initial diameter 100 nm) by nanosecond laser pulses at the wavelength of 532 nm through different kinds of diffusive elements, and compare the UV-vis spectra of colloidal Ag NPs with that irradiated by the laser beam without a diffuser (we call it *normal beam* hereafter). For fairness, the pulse energies of all beams are set to be the same *before* the diffusers. Due to the non-negligible diffusion angles 84, 79, 47, and 60 % of the laser pulse energy can go into the cuvettes when no diffuser, holographic diffuser (#47-988, Edmund Optics), glass diffuser (DG10-1500, Thorlabs), and Scotch tape (3M) are employed, respectively. Note that this

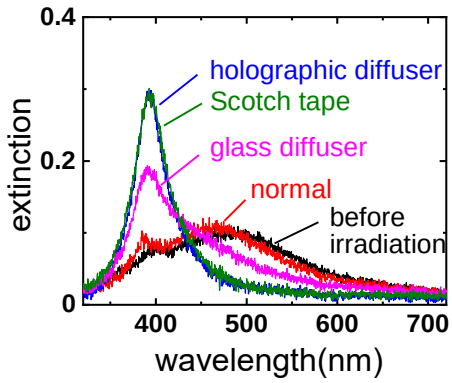


**Figure 1.** UV-vis spectra of the colloidal solution of 100 nm Ag NPs after the 10 min irradiation of 532 nm laser pulses at 15 mJ through different kinds of diffusers.

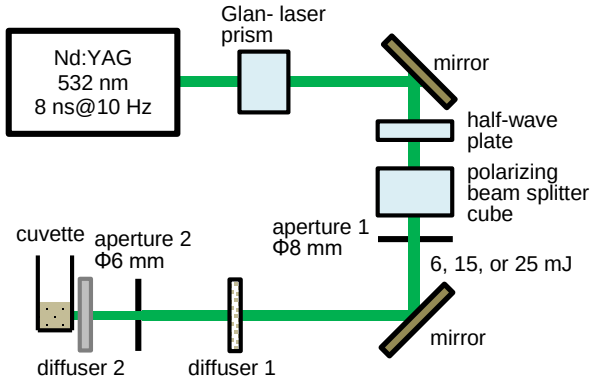


**Figure 2.** Experimental setup. A holographic diffuser is placed at diffuser 1, while a glass diffuser or Scotch tape are placed at diffuser 2, respectively. Note that the pulse energies of 6, 15, and 25 mJ after aperture 1 correspond to the laser fluence of 13, 34, and 56 mJ/cm$^2$ at the cuvette.

pulse energy setup is a more stringent comparison to demonstrate that, in spite of some energy loss caused by the introduction of a diffuser, the use of a diffused laser beam is advantageous to enhance the size-reduction of nanoparticles. diffuser Figure 1 shows the UV-vis spectra of the colloidal Ag NPs after the 10 minutes irradiation at the pulse energy of 15 mJ which is measured before the diffusers. Before laser irradiation the surface plasmon resonance (SPR) of 100 nm Ag NPs is located at around ~490 nm (black curve, figure 1), and the fluence of the normal beam at this pulse energy is so marginal to induce size-reduction of Ag NPs, and only a very small fraction of Ag NPs undergoes size-reduction, as noticed by the small peak at ~380 nm (red curve, figure 1). Very interestingly, the laser beam through a Scotch tape as well as a holographic diffuser turn out to be very efficient to reduce the size of Ag NPs (green and blue curves, figure 1), as we can easily infer from the significant increase of the height of SPR at ~390 nm, and even the laser beam through a glass diffuser which suffers from a wide diffusion angle and accordingly the severe loss of pulse energy works better than the normal beam. Note that the local field enhancement around NPs does not occur in our setup since

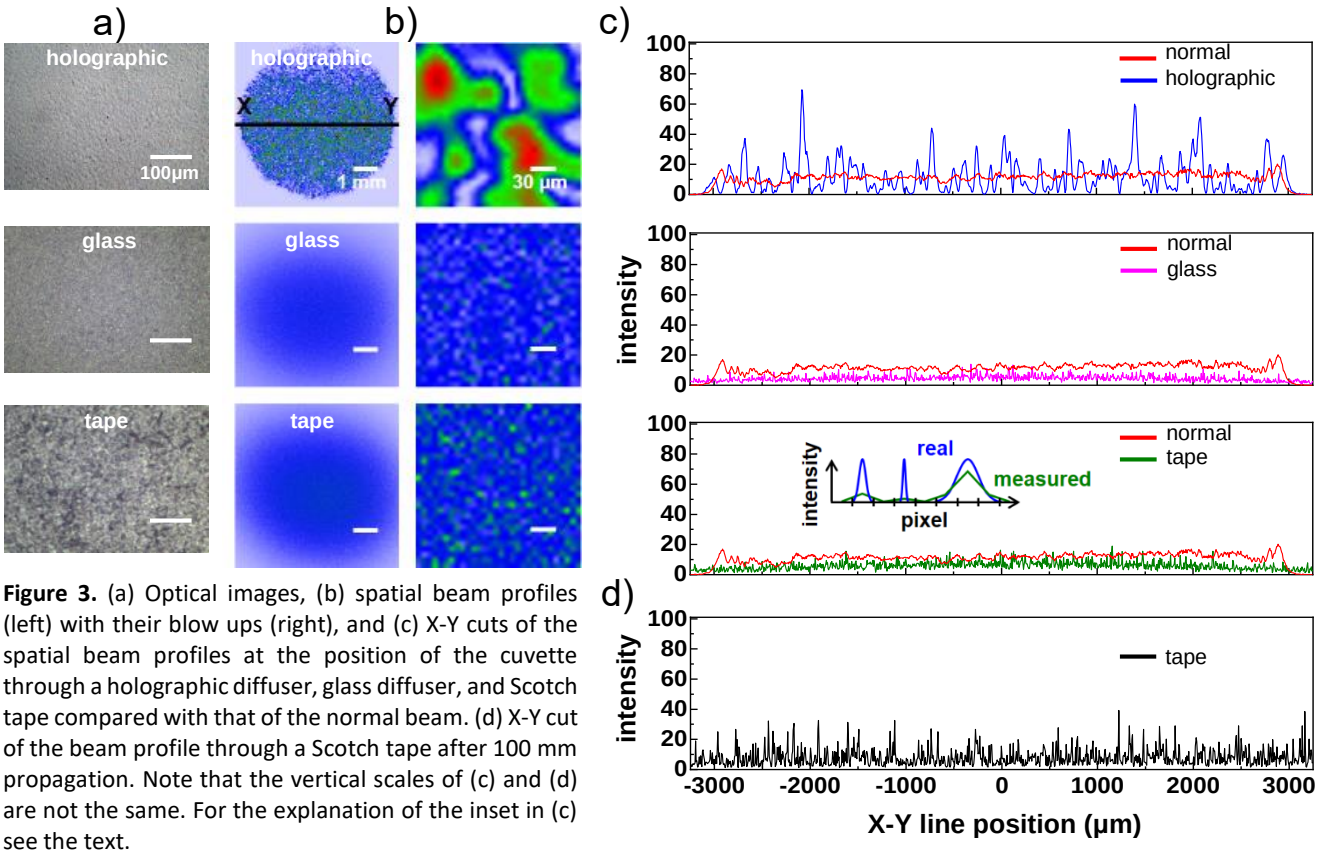


**Figure 3.** (a) Optical images, (b) spatial beam profiles (left) with their blow ups (right), and (c) X-Y cuts of the spatial beam profiles at the position of the cuvette through a holographic diffuser, glass diffuser, and Scotch tape compared with that of the normal beam. (d) X-Y cut of the beam profile through a Scotch tape after 100 mm propagation. Note that the vertical scales of (c) and (d) are not the same. For the explanation of the inset in (c) see the text.

interparticle distance is more than two orders of magnitude larger than the size of nanoparticles.

Given the above intriguing results, the purpose of this paper is to identify the physical origin of the puzzling efficiency of diffused laser beam to reduce the size of Ag NPs, and demonstrate that the qualitatively similar results can be found for other NPs such as gold (Au) NPs.

## 2. Experiments

The experimental setup is shown in figure 2. Colloidal solutions of Ag NPs with diameters of 100, 40, 20, and 10 nm (730777, 730807, 730793, 730785, Sigma-Aldrich) and those of Au NPs with the same diameters (742031, 741981, 741965, 741957, Sigma-Aldrich) are respectively 10 times diluted by deionized water, and 1 mL of the respective diluted colloidal solutions is poured into the quartz cuvette (1 x 1 x 4.5 $cm^3$) which is placed on the magnetic stirrer with a speed of 300 rpm. The second harmonic of an Nd:YAG laser (INDI 30, Spectra Physics, maximum pulse energy 80 mJ at 532 nm, pulse duration 8 ns, repetition rate 10 Hz) goes through the Glan laser prism, half-wave plate, and polarizing beam splitter to adjust the pulse energy. Pulse energies are measured after the first aperture with a diameter of 8 mm, and kept to be the same for both normal and diffused beams. The second aperture with a diameter of 6 mm is placed at 90 mm from the cuvette. As for the position of the diffusers, the holographic diffuser (#47-988, Edmund Optics) is placed at 235 mm from the cuvette, while the glass diffuser (DG10-1500, Thorlabs) and Scotch tape (3M) are placed just in front of the cuvette to avoid the severe beam divergence. The spatial profile of the laser beam is characterized by the beam profiler (BC106-VIS, pixel size of 6.45 x 6.45 $\mu m^2$, Thorlabs) at the position of the cuvette. After laser irradiation the UV-vis spectra of colloidal NPs are measured by the compact CCD spectrometer (USB2000+, Ocean Optics).

To characterize the size distribution of NPs we further dilute the laser-irradiated colloidal solutions 10 times and apply the centrifuge at 2000 rpm for 20 minutes to remove large NPs (presumably original size). Then, we take 2 µL of the supernatant with a microsyringe and drop it on a substrate for the observation with a scanning electron microscope (SEM) (JSM-6500FE, JEOL) at 10 kV. To obtain the particle size distributions we analyze the SEM images with ImageJ.

## 3. Results and Discussions

To start with, we seek for the physical origin of the puzzling efficiency of diffused laser beam to reduce the size of Ag NPs. To find a clue we take the optical images of those diffusive elements with a microscope and measure the spatial profiles of the diffused beams. The results are shown in figure 3.

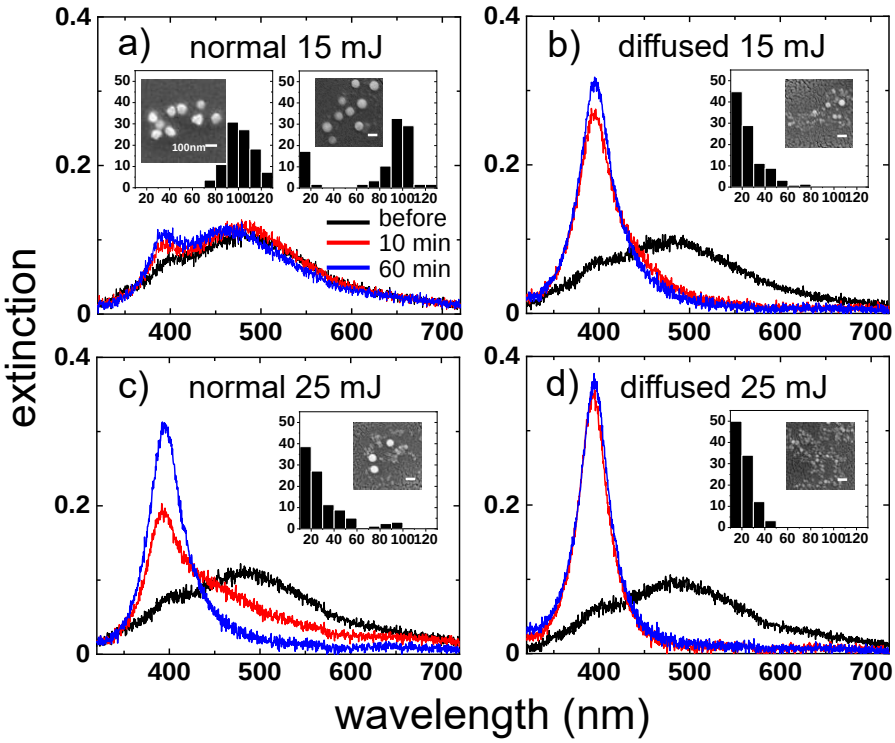


**Figure 4.** UV-vis spectra of the colloidal solutions of initially 100nm Ag NPs before (black), after 10 min (red), and 60 min (blue) irradiation by the (a) normal and (b) diffused beams at 15 mJ. Similar results at the 25 mJ irradiation are presented in (c) and (d), respectively. Insets show the corresponding particle size distributions with horizontal and vertical axes representing the diameter (nm) and fraction (%), respectively, and SEM images, with the left one in (a) being those before laser irradiation while all others after 10 minutes irradiation.

Although the beam profile through the holographic diffuser clearly shows the speckles (blue curve, figure 3 (c)) where the *local* laser fluence can be ~5x of the normal beam which we can identify as the physical origin of the puzzling efficiency, we find no such speckles for the laser beams through the glass diffuser (magenta curve, figure 3 (c)) and Scotch tape (green curve, figure 3 (c)). However, a careful inspection of the beam profile after the propagation distance of 100 mm through the Scotch tape reveals the presence of much finer speckles (figure 3 (d)) than those through the holographic diffuser. This implies that, although very fine speckles are present even for the beam though the Scotch tape, they are too small for the pixel size (6.45 x 6.45 $\mu m^2$) of the beam profiler to be correctly measured at the position of the cuvette. The manual of the employed beam profiler says that the smallest measurable profile is about ~30 μm, which is actually the size of the scale bar of the blow ups in figure 3(b). Accordingly, the measured intensities (widths) of the very fine speckles through the Scotch tape are underestimated (overestimated), and the intensities of the spatially narrower speckles are more severely underestimated, as illustrated in the inset of figure 3(c) for the Scotch tape. The same argument must hold for the beam profile through the glass diffuser. Therefore, regardless of type of the employed diffusive element, figure 3 is a clear evidence that the efficient size-reduction of NPs by the diffused laser beams arises from the redistribution of laser energy around the speckles where the *local* laser fluence exceeds the threshold to induce size-reduction of NPs, i.e., temperature increase of NPs located at the laser speckles is sufficiently high to result in size-reduction. Although the redistribution of laser energy in our case is in the μm regime the above phenomenon is reminiscent of subwavelength light focusing using random NPs [27].

Having identified the physical origin of the high efficiency of diffuse laser beams with different diffusive elements, we employ the holographic diffuser only for all results to be presented in the rest of this paper, since its diffusion angle is very small (0.5 °) with a good pulse energy throughput (79 %), which are similar to those of the normal beam, ~0 ° and 84 %, respectively.

In figure 4 we compare the UV-vis spectra of the colloidal solutions of Ag NPs (initial diameter 100 nm) irradiated by the normal and diffused beams with pulse energies of 15 and 25 mJ measured after the first aperture (aperture 1 in figure 2). Note that those pulse energies correspond to 9.6 and 15.9 mJ after aperture 2 without a diffuser, and hence 34 and 56 $mJ/cm^2$, respectively, for the normal beam. Of course, for the change of fluence and irradiation time the behavior of the UV-vis spectra of the colloidal Ag NPs by the normal beam is similar to those reported earlier [7]. As we see in figure 4(a), the normal beam at 15 mJ can hardly reduce the size of NPs, and even after the 60 minutes irradiation the height of the SPR at ~390 nm remains very small (blue curve, figure 4(a)). In contrast, the diffused beam at the same pulse energy can efficiently reduce the size of NPs, and the SPR at ~390 nm grows much faster and the SPR at ~490 nm almost disappears after 10 minutes (red curve, figure 4(b)). Although the increase of the height of SPR at ~390 nm between 10 and 60 minutes irradiations is not so much, we notice the slight blue shift of the peak (red and blue curves, figure 4(b)). This implies that the overall size of NPs after 60 minutes irradiation is smaller than that after 10 minutes irradiation. When the pulse energy is increased to 25 mJ, however, we see that the normal beam can also induce the size-reduction (figure 4(c)). But it is still less efficient than that by the diffused beam at 15 mJ, as we notice by comparing figure 4(b) and figure 4(c). As expected, the diffused beam at 25 mJ (figure 4(d)) can do the even better job than that of the diffused beam at 15 mJ, not to mention the normal beam at 25 mJ. Note that the width of the peak (height of the tail) of the SPR obtained after 10 as well as 60 minutes irradiation by the diffused beam at 25 mJ are narrower (lower) than those by the diffused beam at 15 mJ, and this indicates that the size of overall NPs after the irradiation of diffused beam at 25 mJ is smaller than that at 15 mJ. The corresponding particle size distributions are shown in the insets of figure 4, and they are consistent with the UV-vis spectra. As we clearly see in figures 4(c) and (d) the use of diffused beam results in not only the higher reduction efficiency but also narrowing the size distribution.

Up to now we have shown the results of colloidal Ag NPs with an initial diameter of 100 nm. A natural question is how the

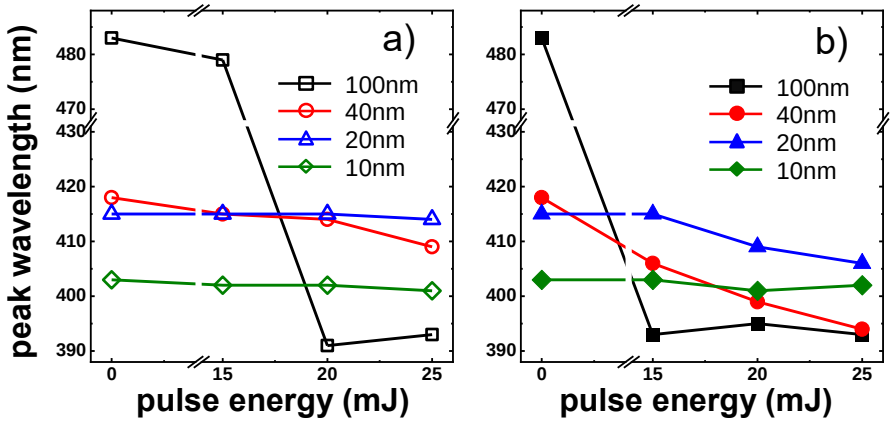


**Figure 5.** Position of the SPR of Ag NPs after 10 minutes irradiation at different pulse energies by the (a) normal and (b) diffused beams. Note that the different colors (symbols) represent the results for the colloidal Ag NPs with different *initial* diameters, 100, 40, 20, and 10 nm.

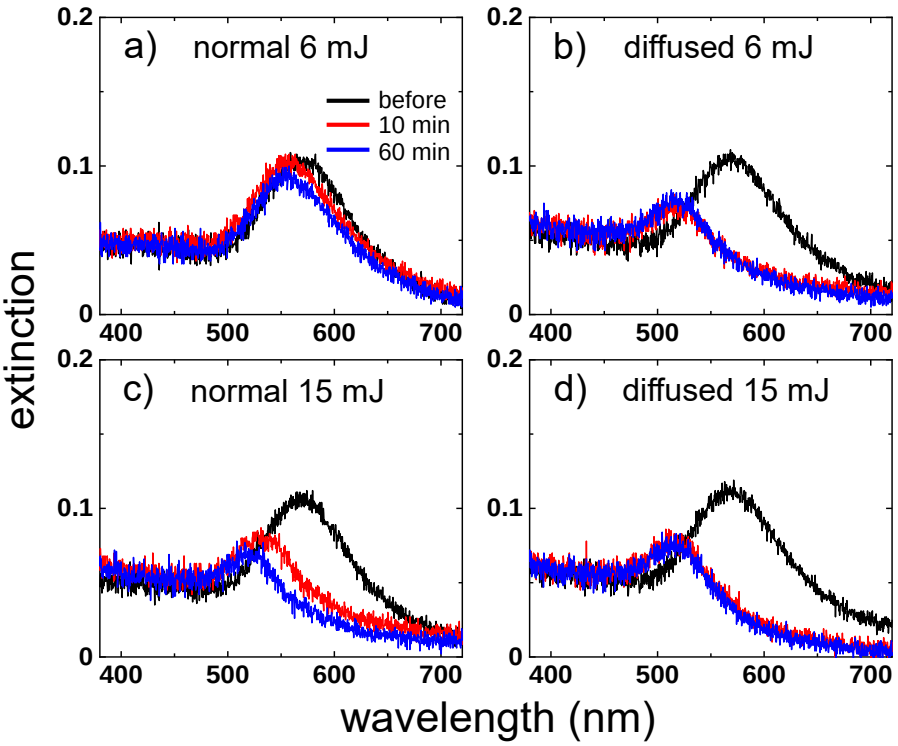


**Figure 6.** UV-vis spectra of the colloidal solutions of initially 100nm Au NPs before (black), after 10 min (red), and 60 min (blue) irradiation by the (a) normal and (b) diffused beams at 6 mJ. Similar results at the 15 mJ irradiation are presented in (c) and (d), respectively.

diffused beam works for NPs with different initial diameters. To answer this question we carry out the similar irradiation experiments for colloidal Ag NPs with initial diameters of 40, 20, and 10 nm, respectively, and plot the change of the peak positions of SPR after 10 minutes irradiation of the normal as well as diffused beams at different pulse energies. Figure 5 summarizes the results. Generally speaking, the diffused beam outperforms the normal beam to reduce the size of Ag NPs with the initial diameters of 100 (as shown in figure 4), 40, and 20 nm. However, the peak position of Ag NPs with an initial diameter of 10 nm hardly changes even at the highest pulse energy we have employed in this work, 25 mJ. Obviously, this is because the absorption cross section of smaller NPs is much smaller than that of the larger ones, and more pulse energy is required to further reduce the size of Ag NPs with 10 nm diameter. The holographic diffuser employed in this work is made by polycarbonate and epoxy resin for the substrate and holographic patterns on it, respectively, and it is not durable for higher laser fluence. Therefore, to use the current technique for a higher laser fluence a similar diffuser made by fused silica (say, #47-680, Edmund Optics) would be more appropriate.

To demonstrate that qualitatively similar results are obtained for other kinds of colloidal NPs, we now employ colloidal Au NPs with an initial diameter of 100 nm, and the results are presented in figure 6. As expected the diffused beam at 6 mJ outperforms the normal beam at the same pulse energy (figures 6(a) and (b)). However, this pulse energy is about 40 % of that for colloidal Ag NPs with the same initial diameter. At the pulse energy of 15 mJ, the difference between the two beams becomes small (figures 6(c) and (d)). Needless to say, the UV-vis spectra of colloidal Au NPs irradiated by the normal beam at the different fluences for the different irradiation times are qualitatively similar to those reported earlier [8,15].

About a factor of three difference in pulse energy to observe the onset of size-reduction of Ag (figure 4) and Au NPs (figure 6) by the normal beam can be well explained by considering the photothermal heating of Ag and Au NPs with a single laser pulse. According to the particle heating-melting-evaporation model [3], the incident laser fluence, $J$, absorption cross section of a nanoparticle, $\sigma_{\text{abs}}(\lambda)$, at a given wavelength, $\lambda$, and the highest temperature of the nanoparticle, $T$, are connected through the following equation:

$$J\sigma_{\text{abs}}(\lambda) = m\left[\int_{T_0}^{T_m} c_p^s(T)dT + \Delta H_m + \int_{T_m}^{T} c_p^l(T)dT\right]$$
$$= m\left[\left(H_{T_m} - H_0\right) + \Delta H_m + \left(H_T - H_{T_m}\right)\right].$$

Note that the heat loss has been completely neglected in the above equation, since it becomes significant in much later time after the laser pulse [3]. Influence of plasmonic nanobubbles [28] that will be produced around nanoparticles is also negligible at the laser fluence in this study. $c_s(T)$ and $c_l(T)$ are the heat capacities of the NP in solid and liquid phases, $m$ is NP's mass, while $T_0$, $T_m$, and $T_b$ are the initial, melting, and boiling temperatures of NP, respectively. $\Delta H_m$ is the enthalpy of melting and $H_{T_m} - H_0$ is the relative enthalpy. All those

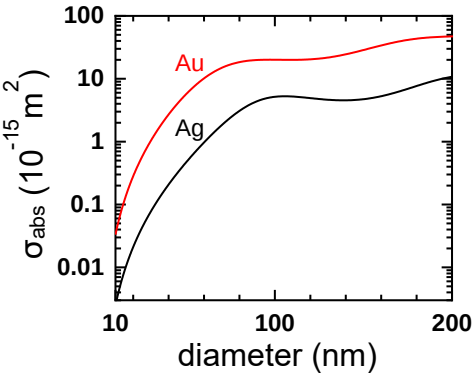


**Figure 7.** Absorption cross section of Ag and Au NPs at 532 nm as a function of particle diameter calculated by the Mie's theory [28].

parameters are listed in the literature [3]. Among all the parameters that affect the temperature of Ag and Au NPs, the most striking difference can be seen in the absorption cross section, and using the Mie's theory [29] we calculate the absorption cross section of Ag and Au NPs as a function of particle diameter. The results are shown in figure 7, and we find that the absorption cross sections of Ag NPs at 532 nm are 2.55 $\times$ $10^{-18}$, 2.10 $\times$ $10^{-17}$, 2.06 $\times$ $10^{-16}$ and 5.18 $\times$ $10^{-15}$ $m^2$, respectively, for the diameters of 10, 20, 40, and 100 nm. As mentioned before, the pulse energy 25 mJ (at aperture 1, figure 2) corresponds to 56 mJ/$cm^2$ (at the cuvette) for the normal beam. Using the above equation together with the absorption cross sections of Ag NPs and laser fluences we find that the highest temperature of 10, 20, 40, and 100 nm Ag NPs after the single-shot normal beam irradiation at 25 mJ (56 mJ/$cm^2$) are 1234, 1234, 1234, and 1800 K. Since the melting and boiling points of bulk Ag are 1234 and 2437 K, we can say that the laser-induced size-reduction by the normal beam at 25 mJ occurs for 100 nm Ag NPs, while it marginally (hardly) occurs for 40 nm (10 and 20 nm) NPs. Similarly, knowing the absorption cross section of 100 nm Au NPs at 532 nm is 2.00$\times$$10^{-14}$ $m^2$ from figure 7, the highest temperatures of 100 nm Au NPs after the single-shot irradiation at 6 and 15 mJ (13 and 34 mJ/$cm^2$) are calculated to be 1620 and 3108 K, respectively, which are to be compared with the melting and boiling points of bulk Au, 1336 and 3108 K. The above estimation of the highest temperature of 100 nm Ag and Au NPs explains why the onset of size-reduction of Au NPs with a diameter of 100 nm is about 6 mJ while that of Ag NPs is about 15 mJ. Those temperature estimations of Ag and Au NPs irradiated by the normal beam with different laser fluences well explain why the diffused beam can do the better job to reduce the size of Ag and Au NPs.

## 4. Conclusions

In conclusion we have demonstrated that a diffused laser beam is more efficient to induce the size-reduction of silver and gold nanoparticles than the non-diffused (i.e., nearly flat-top) laser beam with the same pulse energy and diameter. We have identified that the physical origin of the puzzling efficiency of diffused laser beam is the redistribution of laser energy so that the local laser fluence exceeds the size-reduction threshold. Thus, the demonstrated technique should be applicable to any NPs and NRs for size-reduction, reshaping, welding, etc., for which there exist laser flunce thresholds to induce the desired processes. Indeed, we have confirmed that the diffused laser beam also works well for the size-reduction of gold NPs. Altering the spatial profile of a laser beam can be a new door-knob to enhance laser-nanoparticle interactions.

**Disclosures.** The authors declare no conflicts of interest.

## References


[1] Zeng H, Du X W, Singh S C, Kulinich S A, Yang S, He J and Cai W 2012 Nanomaterials via laser ablation/irradiation in liquid: A review *Adv. Funct. Mater.* **22** 1333–53

[2] Zhang D, Gökce B and Barcikowski S 2017 Laser Synthesis and Processing of Colloids: Fundamentals and Applications *Chem. Rev.* **117** 3990–4103

[3] Pyatenko A, Wang H, Koshizaki N and Tsuji T 2013 Mechanism of pulse laser interaction with colloidal nanoparticles *Laser Photonics Rev.* **7** 596–604

[4] Besner S, Kabashin A V., Winnik F M and Meunier M 2008 Ultrafast laser based "green" synthesis of non-toxic nanoparticles in aqueous solutions *Appl. Phys. A Mater. Sci. Process.* **93** 955–9

[5] Al-Mamun S A, Nakajima R and Ishigaki T 2013 Tuning the size of aluminum oxide nanoparticles synthesized by laser ablation in water using physical and chemical approaches *J. Colloid Interface Sci.* **392** 172–82

[6] Giorgetti E, Marsili P, Cicchi S, Lascialfari L, Albiani M, Severi M, Caporali S, Muniz-Miranda M, Pistone A and Giammanco F 2015 Preparation of small size palladium nanoparticles by picosecond laser ablation and control of metal concentration in the colloid *J. Colloid Interface Sci.* **442** 89–96

[7] Takami A, Yamada H, Nakano K and Koda S 1996 Size Reduction of Silver Particles in Aqueous Solution by Laser Irradiation *Japanese J. Appl. Physics, Part 2 Lett.* **35** L781–3

[8] Kurita H, Takami A and Koda S 1998 Size reduction of gold particles in aqueous solution by pulsed laser irradiation *Appl. Phys. Lett.* **72** 789–91

[9] Takami A, Kurita H and Koda S 1999 Laser-induced size reduction of noble metal particles *J. Phys. Chem. B* **103** 1226–32

[10] Yamada K, Tokumoto Y, Nagata T and Mafuné F 2006 Mechanism of laser-induced size-reduction of gold nanoparticles as studied by nanosecond transient absorption spectroscopy *J. Phys. Chem. B* **110** 11751–6

[11] Muto H, Miyajima K and Mafuné F 2008 Mechanism of laser-induced size reduction of gold nanoparticles as studied by single and double laser pulse excitation *J. Phys. Chem. C* **112** 5810–5

[12] Pyatenko A, Yamaguchi M and Suzuki M 2009 Mechanisms of size reduction of colloidal silver and gold nanoparticles irradiated by Nd:YAG laser *J. Phys. Chem. C* **113** 9078–85

[13] Werner D, Furube A, Okamoto T and Hashimoto S 2011 Femtosecond laser-induced size reduction of aqueous gold nanoparticles: In situ and pump-probe spectroscopy investigations revealing coulomb explosion *J. Phys. Chem. C* **115** 8503–12

[14] Akman E, Aktas O C, Genc Oztoprak B, Gunes M, Kacar E, Gundogdu O and Demir A 2013 Fragmentation of the gold nanoparticles using femtosecond Ti:Sapphire laser and their structural evolution *Opt. Laser Technol.* **49** 156–60

[15] Inasawa S, Sugiyama M and Yamaguchi Y 2005 Laser-induced shape transformation of gold nanoparticles below the melting point: The effect of surface melting *J. Phys. Chem. B* **109** 3104–11

[16] Kamat P V., Flumiani M and Hartland G V. 1998 Picosecond dynamics of silver nanoclusters. Photoejection of electrons and fragmentation *J. Phys. Chem. B* **102** 3123–8

[17] Giammanco F, Giorgetti E, Marsili P and Giusti A 2010 Experimental and theoretical analysis of photofragmentation of au nanoparticles by picosecond laser radiation *J. Phys. Chem. C* **114** 3354–63

[18] Wang H, Pyatenko A, Kawaguchi K, Li X, Swiatkowska- Warkocka Z and Koshizaki N 2010 Selective pulsed heating for the synthesis of semiconductor and metal submicrometer spheres *Angew. Chemie - Int. Ed.* **49** 6361–4

[19] Ishikawa Y, Koshizaki N, Pyatenko A, Saitoh N, Yoshizawa N and Shimizu Y 2016 Nano- and Submicrometer-Sized Spherical Particle Fabrication Using a Submicroscopic Droplet Formed Using Selective Laser Heating *J. Phys. Chem. C* **120** 2439–46

[20] Link S, Burda C, Nikoobakht B and El-Sayed M A 2000 Laser-induced shape changes of colloidal gold nanorods using femtosecond and nanosecond laser pulses *J. Phys. Chem. B* **104** 6152–63

[21] Ishikawa Y, Shimizu Y, Sasaki T and Koshizaki N 2006 Preparation of zinc oxide nanorods using pulsed laser ablation in water media at high temperature *J. Colloid Interface Sci.* **300** 612–5

[22] González-Rubio G, Guerrero-Martínez A and Liz-Marzán L M 2016 Reshaping, Fragmentation, and Assembly of Gold Nanoparticles Assisted by Pulse Lasers *Acc. Chem. Res.* **49** 678–86

[23] Kuladeep R, Jyothi L, Alee K S, Deepak K L N and Rao D N 2012 Laser-assisted synthesis of Au-Ag alloy nanoparticles with tunable surface plasmon resonance frequency *Opt. Mater. Express* **2** 161

[24] Semaltianos N G, Hendry E, Chang H, Wears M L, Monteil G, Assoul M, Malkhasyan V, Blondeau-Patissier V, Gauthier-Manuel B and Moutarlier V 2016 Ns or fs pulsed laser ablation of a bulk InSb target in liquids for nanoparticles synthesis *J. Colloid Interface Sci.* **469** 57–62

[25] Amendola V, Scaramuzza S, Carraro F and Cattaruzza E 2017 Formation of alloy nanoparticles by laser ablation of Au/Fe multilayer films in liquid environment *J. Colloid Interface Sci.* **489** 18–27

[26] Dai S, Li Q, Liu G, Yang H, Yang Y, Zhao D, Wang W and Qiu M 2016 Laser-induced single point nanowelding of silver nanowires *Appl. Phys. Lett.* **108** 1–6

[27] Park J H, Park C, Yu H, Park J, Han S, Shin J, Ko S H, Nam K T, Cho Y H and Park Y 2013 Subwavelength light focusing using random nanoparticles *Nat. Photonics* **7** 454–8

[28] Nakajima T, Wang X, Chatterjee S and Sakka T 2016 Observation of number-density-dependent growth of plasmonic nanobubbles *Sci. Rep.* **6** 1–9

[29] Laven P A computer program for scattering of light from a sphere using Mie theory & the Debye series